

Vehicle model simulation to predict the judder vibration reduction performance of hydraulic bushing

Won Park^{1*}, Kwangseok Boo² and Heungseob Kim³

¹ Mechanical Engineering
Inje University, 50834 Gimhae, Gyeongnam, Korea
pw5277@hanmail.net

² HSV-TRC Center
Inje University, 50834, Gimhae, Gyeongnam, Korea
mechboo@inje.ac.kr

³ HSV-TRC Center
Inje University, 50834, Gimhae, Gyeongnam, Korea
mechhsk@inje.ac.kr

Keywords: Judder, Hydraulic bushing, Loss Angle, Dynamic Stiffness

Abstract. Generally, judder vibration is a low-frequency vibration phenomenon caused by a braking force imbalance that occurs when a vehicle is lightly decelerated within a range of 0.1 to 0.2g at a speed of 120 to 60 km/h. This comes from the change in the brake disk thickness (DTV), which is mainly caused by the side run-out (SRO) and thermal deformation. The adoption of hydro-bushing in the low arm G bushings of the vehicle front suspension has been done in order to provide great damping in a particular frequency range (<20Hz) in order to prevent this judder vibration from being transmitted to the body. The hydro bushing was formulated using a lumped parameter model. The fluid passage between the two chambers was modelled as a nonlinear element such as an orifice, and its important parameters (resistance, compliance) were measured using a simplified experimental setup. The main design parameters are the ratio of the cross-sectional area of the chamber to the fluid passage, the length of the fluid passage, etc., and their optimal design is such that the loss angle is greater than 45 ° in the target frequency range of 10 to 20 Hz. The hydro bushing designed for reducing the judder vibration was prepared for the actual vehicle application test and applied to the actual vehicle test. In this study, the proposed hydro bushing was applied to the G bushing of the low arm of the front suspension system of the vehicle. The loss angle of the manufactured hydro bushing was measured using acceleration signals before and after passing through the bushing. The actual vehicle test was performed on the noise dynamometer for the performance analysis of the judder vibration reduction.

1 INTRODUCTION

Generally, in vibration theory, it is known that high stiffness and large damping are easy to cut off low frequency and large displacement vibration, low stiffness and small damping are advantageous for high frequency and small displacement vibration.

The conventional rubber bushing meets the contradictory requirements of sufficient attenuation for large displacement vibrations in the rigid body mode below 100 Hz and high

decoupling of the structural noise in the high frequency range. The requirements of this contradictory bushing design have required the development of hydrobushing which can enhance the damping force through the fluid and control the stiffness and damping in the frequency range of interest. The principle of fluid damping technology is already known in engine mount technology, but there are constraints in design and material selection for application in chassis components. Nevertheless, the suspension application of the hydrobushing was applied to the lower arm G bushing of the front suspension in Fig.1 to reduce the steering wheel judder vibration due to the braking force imbalance. [1~2]

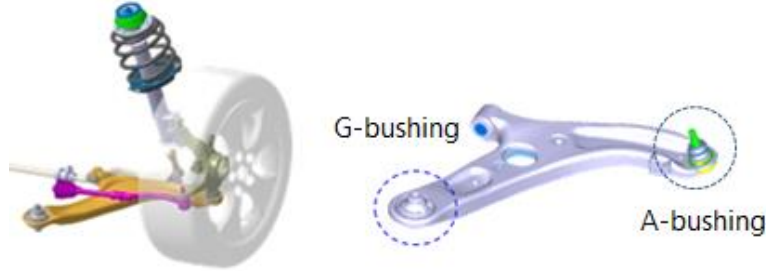


Figure 1. G bushing position of lower arm in the MacPherson suspension

Judder vibration is a low-frequency vibration phenomenon in the range of 10 ~ 20Hz caused by unbalance of braking force when the vehicle is braking at a light deceleration of 0.1 ~ 0.2g at a speed of 120km/h, which is a highway driving speed. Judder is known to be caused by disc thickness variation (DTV), which is caused by side run-out (SRO) during manufacturing and thermal deformation resulting from the braking process. Compared to conventional rubber bushings, hydro bushings can have high viscous damping in certain frequency ranges, but have amplitude and frequency dependencies. The design core of the hydro bushing is to determine the peak frequency and magnitude of the loss angle. The main design parameters are rubber spring constant, fluid characteristics, and the shape of the chamber and inertia track.

In this study, the frequency characteristics of the hydro bushing applied to the G bushing of the front suspension low arm were designed to effectively reduce the judder vibration. Also, the performance of the hydro bushing was verified by performing the actual vehicle test on the noise dynamo using the vehicle with the hydro bushing manufactured.

2 Characteristic design of hydrobushing

The lumped parameter model (LP model) as shown in Fig.2 is widely used to predict the characteristic analysis of the hydrobushing [3~4]. The hydro bushing consists of two chambers connected by fluid passages, rubber elements and a metal sleeve on the inside and on the opposite side. The rubber elements consist of a Kelvin-Voigt model with frequency-invariant stiffness K_R and viscous damping coefficient C_R . The two chambers are defined by compliance C_1 , C_2 controlled by the rubber portion and the fluid portion including the air. The fluid passage is modeled by a resistance element R_i and an inertance element I_i .

When dynamic displacement is applied to the inner sleeve of the hydrobushing, the dynamic pressure of both chambers is

$$C_1 \dot{p}_1(t) = -A_1 \dot{x}(t) - q_i(t) \quad (1)$$

$$C_2 \dot{p}_2(t) = A_2 \dot{x}(t) + q_i(t) \quad (2)$$

Where A_1, A_2 represents the effective pumping area of each chamber, and q_i represents the volumetric flow rate of the fluid flowing through the fluid passages connecting the chambers. The conservation of momentum between the chamber and the fluid passage can be expressed as Equation (3).

$$p_1(t) - p_2(t) = I_i \dot{q}_i(t) + R_i q_i(t) \quad (3)$$

The forces transmitted by the two paths to the outer sleeve are as follows.

$$f_T(t) = [C_R \dot{x}(t) + K_R x(t)] + [A_2 p_2(t) - A_1 p_1(t)] \quad (4)$$

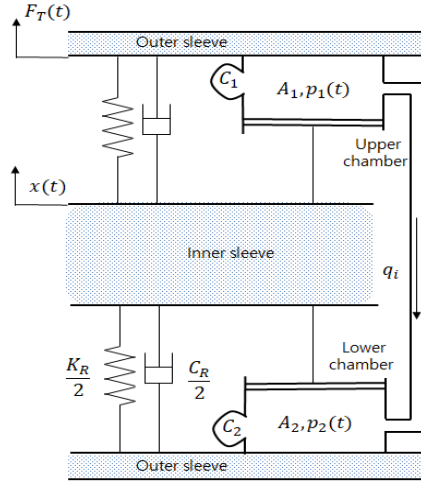


Figure 2. Lumped parameter model of hydrobushing

The resistance $R_i(q_i)$ of the fluid passage can be modeled nonlinearly using the same orifice model as Eq. (5) [5].

$$R_i(q_i) = \frac{\Delta p}{q_i} = \lambda \frac{\rho}{2A_i C_d^2} |q_i(t)| = c_R |q_i(t)| \quad (5)$$

Where C_d is the expansion coefficient, A_i is the cross-sectional area of the fluid passage, and c_R is the resistance coefficient. λ is a coefficient that adjusts the difference between experimental and theoretical models. The hydro bushing with nonlinear characteristics for sinusoidal input is tried to obtain the transfer function for the dynamic stiffness and loss angle. If the fluid channel is made nonlinear as shown in Eq. (5), Eq. (3) becomes as shown in Eq. (6). If the two chambers have the same cross-sectional area, Eq. (7) can be obtained by combining Eq. (1) and Eq. (2).

$$p_1(t) - p_2(t) = I_i \dot{q}_i(t) + c_R |q_i(t)| q_i(t) \quad (6)$$

$$I_i \ddot{q}_i(t) + 2c_R q_i(t) \dot{q}_i(t) \text{sgn}[q_i(t)] + k q_i(t) = \alpha_x \dot{x}(t) \quad (7)$$

Where $k = 1/C_1 + C_2$, $\alpha_x = - [A_1/C_1 + A_2/C_2]$. Assuming that the input displacement of the hydrobushing inner sleeve is $x(t) = X \sin(\omega t - \varphi)$, and the flow rate of the resulting hydraulic passage is $q(t) = Q_I \sin(\omega t)$, then Eq. (7) is

$$\begin{aligned} kQ_1 \sin(\omega t) + c_R Q_1^2 \omega \sin(2\omega t) \operatorname{sgn}[\sin(\omega t)] - I\omega^2 Q_1 \sin(\omega t) \\ = \alpha_x X \omega [\cos(\omega t) \cos \varphi + \sin(\omega t) \sin \varphi] \end{aligned} \quad (8)$$

Eq. (8) can be simplified by using the Fourier series for $\sin(2\omega t) \operatorname{sgn}[\sin(2\omega t)]$, as shown in Eq. (9).

$$\varphi = \tan^{-1} \frac{\sqrt{2}(k - I\omega^2)}{\sqrt{-(k - I\omega^2)^2 + \sqrt{(k - I\omega^2)^4 - 4 \left(\frac{8\alpha_x X c_R \omega^2}{3\pi} \right)^2}}} \quad (9)$$

$$Q_1^2 = \frac{-(k - I\omega^2)^2 + \sqrt{(k - I\omega^2)^4 - 4 \left(\frac{8\alpha_x X c_R \omega^2}{3\pi} \right)^2}}{\frac{2(8c_R \omega)^2}{(3\pi)^2}} \quad (10)$$

The flow rates in Eq. (9) and Eq. (10) are as follows.

$$Q(\omega) = Q_1 \cos \varphi + i Q_1 \sin \varphi \quad (11)$$

And the dynamic stiffness and loss angle can be obtained by Eq. (4).

$$K_d(\omega) = K_R + i\omega C_R + \gamma + \left(\frac{A_1}{C_1} + \frac{A_2}{C_2} \right) \frac{Q(\omega)}{iX\omega} \quad (12)$$

In Eq. (12), the magnitude and phase of $K_d(\omega)$ correspond to the tangent and loss angles, respectively.

3 Simulation for predicting the performance characteristics

A simulation for predicting the dynamic stiffness and loss angle of hydro bushings with nonlinear elements such as fluid passages was performed. The developed hydro bushing is designed to reduce judder vibration caused by instability caused by friction during braking process. It is designed to have a loss angle of 30 ° or more in the frequency range of 10 ~ 20Hz.

3.1 Design parameters

The developed hydro bushing is shown in Fig. 3. The damping force generated during the flow of the fluid due to the long fluid passage is utilized. Table 1 shows the main design parameters of the hydrobushing. The design is designed to maximize the loss angle in the frequency range of the judder oscillation through the optimal combination of fluid passages and chambers.

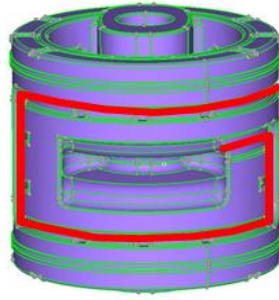


Figure 3. Developed hydrobushing with long flow passage

Table 1. Geometric and material properties

| Part | Parameter | Value |
|---------------|--|--------|
| Rubber | Spring constant, [N/mm] | 430 |
| | Damping coefficient, [Ns/mm] | 0.1 |
| Inertia track | Length, [mm] | 532.1 |
| | Cross sectional area, [mm ²] | 8.4 |
| Chamber | Pumping area, [mm ²] | 5609 |
| Fluid | Viscosity, [Ns/mm ²] | 2.5e-8 |
| | Density, [Ns ² /mm ⁴] | 1.1e-9 |

3.2 Frequency characteristics

The characteristics of the hydrobushing were obtained by increasing the sinusoidal amplitude of 1 mm to 5~ 50Hz at intervals of 1Hz and measuring the dynamic stiffness and loss angle at each frequency. The results are compared with those predicted by Eq. (12), and the comparison results are shown in Fig. 4. In Fig. 4(a), the predicted results for the dynamic stiffness differ from the experimental values in the region above 15 Hz, but the prediction of the loss angle in Fig. 4(b) accurately predicts the position and the value of the maximum loss angle. Therefore, it was confirmed that the algorithm for predicting the hydro-bushing dynamic characteristics was accurately created.

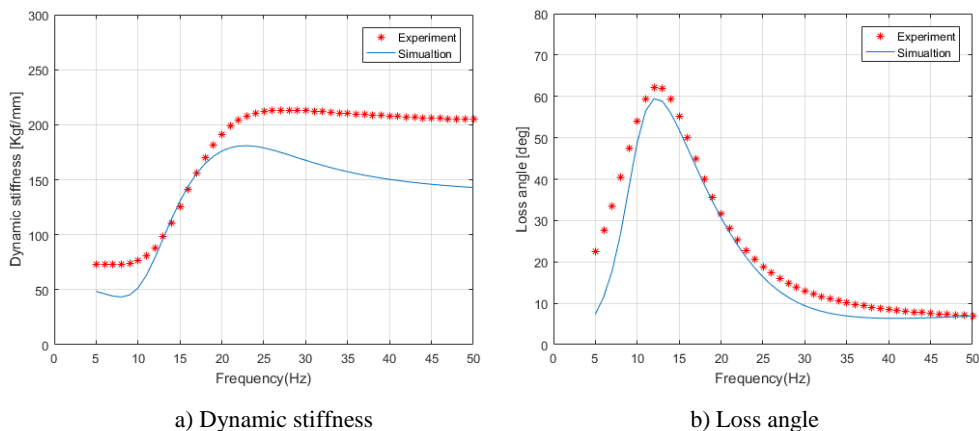


Figure 4. Comparisons between experimental and predicted results of the dynamic characteristics

4 CONCLUSIONS

- In order to predict the accurate dynamic performance of the hydrobushing modeled by the lumped parametric model, this study conducted a measurement experiment on the resistance of the fluid passages and chamber compliance with nonlinear characteristics and reflected them in the prediction algorithm. It is found that the predicted results for the dynamic stiffness and loss angles can predict the peak frequency and magnitude accurately with experimental results. Especially, it was confirmed that a large loss angle value was obtained in a desired frequency range so as to reduce the judder vibration.

ACKNOWLEDGEMENT

This research was supported by the Ministry of Trade, Industry & Energy (MOTIE), Korea Institute for Advancement of Technology (KIAT) through the Encouragement Program for The Industries of Economic Cooperation Region. (R0004519). This research was supported by The Leading Human Resource Training Program of Regional Neo industry through the National Research Foundation of Korea (NRF) funded by the Ministry of Science, ICT and future Planning. (2016H1D5A1910490)

REFERENCES

- [1] W. Sauer, Y. Guy, SAE 2003-01-1475, (2003)
- [2] L. Min, T. Youngjun, and W. Enjung, SAE 2010-01-0506, (2010)
- [3] T. Chai, J. T. Dreyer, and R. Singh, Mechanical Systems and Signal Processing, 56, 92 (2015)
- [4] W. B. Shangguan, C. Xu, Journal of Vibration and Shock, 26, 7 (2007)
- [5] T. Chai, R. Singh, and J. Dreyer, SAE 2013-01-1924 (2013)